

Internal friction study of a composite with a negative stiffness constituent

T. Jaglinski

Materials Science Program, University of Wisconsin—Madison, Madison, Wisconsin 53706-1687

D. Stone^{a)}

Materials Science Program and Department of Materials Science, University of Wisconsin—Madison, Madison, Wisconsin 53706-1687

R.S. Lakes^{b)}

Department of Engineering Physics, Engineering Mechanics Program, Biomedical Engineering Department, Materials Science Program, and Rheology Research Center, University of Wisconsin—Madison, Madison, Wisconsin 53706-1687

(Received 24 February 2005; accepted 31 May 2005)

Composites with negative stiffness constituents can exhibit material properties that exceed conventional bounds. Composites with VO₂ as negative stiffness inclusions and tin as the stabilizing matrix were prepared via powder metallurgy. Specimens were tested over a range of temperature in torsion using broadband viscoelastic spectroscopy. Composites processed via powder metallurgy exhibited internal friction anomalies over a broad range of temperatures, in contrast to the single, sharp anomalies reported previously from cast specimens. The detailed material behavior encompassed a variety of responses, which were also dependent on the number of thermal cycles. Composite theory predictions assuming a distribution of negative shear moduli can account for peak broadening.

I. INTRODUCTION

Most composite morphologies utilize inclusion shapes such as particles, fibers, or platelets etc., to stiffen or strengthen a matrix material. As a consequence of the specific microstructure chosen, the resulting composite material has effective properties intermediate between the base constituents. In the search for novel materials to enhance technological applications over traditional materials, utilization of the negative stiffness concept is one avenue to exceed the usual theoretical bounds placed upon linear, isotropic composites. Composites which contain a negative stiffness phase can theoretically possess properties, specifically modulus and mechanical damping, in excess of those of the base constituents as a result of balance between elements of positive and negative stiffness.

Negative stiffness is manifested by the reversal of the usual directional relationship between causal forces and ensuing deformations and is unstable unless constrained. Negative stiffness differs from negative Poisson's ratio,¹ which refers to the transverse deformation of a material

due to a longitudinal load. The concept of negative stiffness can be illustrated by a set of linear elastic springs, all of which have positive stiffness, arranged into the geometry shown in Fig. 1. In the unloaded, unstretched condition of Fig. 1(a), all applied displacements and subsequent forces to point a will be resisted by the two springs marked k_1 and the third spring marked k_2 . A negative stiffness situation can be obtained by applying enough displacement to point a, forcing the springs into the unstable equilibrium configuration shown in Fig. 1(b). If k_2 is small, this situation is unstable because a perturbation of point b away from k_2 will cause the system to snap to the condition of Fig. 1(c). The so called "snap-through" phenomenon is indicative of negative stiffness and can be visualized by the fact that small applied displacements once the unstable regime of Fig. 1(b) has been reached, result in large structural deformations in the direction of the applied displacement. It must be noted that without the restoring force of spring k_2 attached to a hard, displacement controlled constraint, the unstable, preloaded k_1 springs would simply snap through. Furthermore, if the restoring force of k_2 is sufficiently large snap-through will be suppressed, allowing negative stiffness to be measured in displacement control. Proper balance between the negative and positive elements is required for singular properties.

Address all correspondence to these authors.

^{a)}e-mail: dstone@engr.wisc.edu

^{b)}e-mail: lakes@engr.wisc.edu

DOI: 10.1557/JMR.2005.0316

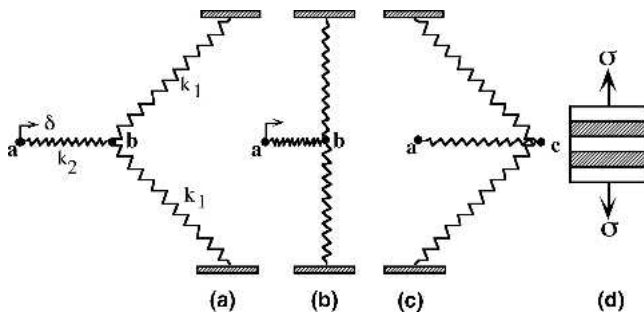


FIG. 1. Combination of linear elastic springs showing negative stiffness from (a) the unstretched condition to (b) the preloaded and unstable configuration to (c) snap-through to the new stable position. As a comparison, (d) shows the Reuss composite, essentially springs in series, which can show extreme composite behavior if one of the composite phases is allowed to have negative stiffness.

The pedagogical idea behind the series spring geometry of Figs. 1(a)–1(c) can be extrapolated to a composite material system such as the Reuss composite [Fig. 1(d)]. This composite is composed of alternating layers of linear elastic materials, which are analogous to springs in series. In this case, one phase is allowed to have negative stiffness while the other positive stiffness phase provides a stabilizing constraint. It has been shown that the inherent structural instability in a Reuss type composite containing a negative stiffness phase can be stabilized by physical constraint, as demonstrated in an experiment with post-buckled tubes by Lakes.² Besides demonstrating the existence of negative structural stiffness in this system, Lakes² further showed increased mechanical damping orders of magnitude larger than that of the tube material. The essence of Lakes's analysis can be understood by examination of the Reuss formula for the effective composite modulus, shown here as Eq. (1)

$$\frac{1}{E_c} = \frac{V_1}{E_1} + \frac{V_2}{E_2} \quad (1)$$

Here, E_c is the effective composite modulus, and E_1 , E_2 , V_1 , and V_2 are the elastic modulus and volume fractions of phase 1 and 2, respectively. If one of the phases is allowed to have a negative modulus, the effective composite modulus can be made arbitrarily large by proper adjustment of V_1 and V_2 . Peaks in the internal friction of a Reuss composite can be found by application of the viscoelastic correspondence principle to Eq. (1).

In practice, a real composite system is not this simple and one must work with a more general, three-dimensional composite system, such as the isotropic, linear elastic composite described by the Hashin–Shtrikman formulas for a composite comprised of coated spheres³ [see Eq. (2) in Sec. IV]. For such a composite, each inclusion is surrounded by a positive stiffness matrix material. Using the matrix instead of a hard boundary as the stabilizing force allows the inclusion elastic modulus

to become negative. Negative moduli, which are allowed by the assumptions of strong ellipticity in linear elasticity, have been shown by Lakes and Drugan³ to be a pathway to extreme composite mechanical behavior. For example, one can have singularities or increases of orders of magnitude in composite modulus or internal friction.

Even though negative moduli are allowed within the framework of linear elasticity, real materials must be used when creating composites with a negative stiffness phase. Negative stiffness can be obtained through ferroelastic phase transformations⁴ or structural phase transformations associated with temperature induced shape change. In this case, negative stiffness is understood within the context of Landau theory as the emergence of a double well, and thus a negative energy gradient, in the order parameter potential as the material is cooled below a critical temperature. One example of a real material system that possesses these characteristics is vanadium dioxide (VO_2), which undergoes a tetragonal to monoclinic ferroelastic transformation at 68 °C. As mentioned, negative stiffness behavior can only be observed in a constrained system. It follows then that negative stiffness VO_2 inclusions must be incorporated into a positive stiffness matrix. In this way, a composite with interesting properties can be created.

Lakes et al.⁵ manufactured a cast Sn– VO_2 composite system where dispersion of the VO_2 inclusions was achieved during solidification of the tin matrix. The VO_2 particles served as the negative stiffness phase and cast tin served as the stabilizing, positive stiffness matrix. Consistent with predictions from composite theory,³ Lakes et al. were able to show that the composite displayed both increases in mechanical damping and anomalies in stiffness inside the temperature window of the phase transformation of VO_2 (Fig. 2). In these

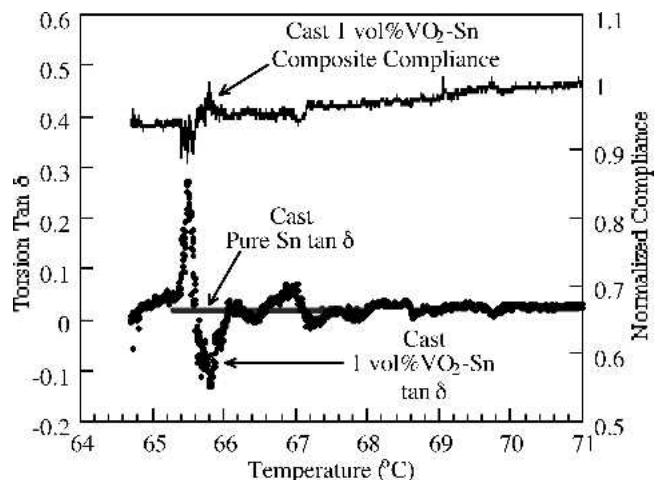


FIG. 2. Experimental data from a 1 vol% VO_2 -SN cast composite. Notice the large spike in $\tan \delta$, and the smaller, but similar, behavior in composite compliance. After Lakes et al.⁵

experiments, negative stiffness was inferred from observed behavior rather than measured directly.

In the original work, particulate inclusions of VO_2 were incorporated into the tin matrix by cold rolling sheets of tin with particles, followed by casting into a cylindrical mold.⁶ However, a rapid heating and cooling process was crucial to the achievement of a successful composite because the less dense VO_2 ($\sim 4.3 \text{ g/cm}^3$) will segregate out of the tin ($\sim 7.31 \text{ g/cm}^3$) if given time to do so. Because of the difficulties involved with sample preparation, systematic titration of phase fractions was not conducted. The powder metallurgy processing technique used in the present study for composite synthesis has the ability to create dispersions of normally immiscible phases and allows tight control of phase volume fractions.

The main thrust of the present work is to study the effect of volume fraction and thermal cycling on the mechanical behavior of Sn-VO_2 composites produced through powder metallurgy. In principle, singular mechanical properties can be obtained in composites with inclusions having negative stiffness. Details regarding the requirements for extreme behavior and the stability criteria for the overall composite are both aspects which are under theoretical investigation.

II. EXPERIMENTAL METHODS

A. Composite preparation and microstructure analysis

Tin powder of 99.8% metal basis and 325 mesh ($\sim 45 \mu\text{m}$, in diameter) and VO_2 powder of 99% metal basis and 100 mesh ($\sim 145 \mu\text{m}$ particle size or less) were obtained from Alfa Aesar (Ward Hill, MA). To create 0, $\frac{1}{2}$, 1, and 5 vol% VO_2 -Sn composites, appropriate masses of each constituent were measured using an electronic balance, hand mixed, and then consolidated in lots of about 20 g total mass.

Consolidation of the powder was carried out in a steel compression die with one movable punch having die dimensions of $50 \times 12 \text{ mm}$. A Carver hydraulic press was used to apply 106 kN of force, corresponding to a nominal compressive stress of about 180 MPa. Powders were both cold and hot pressed. When cold pressed, the green compact was sintered in an argon atmosphere, which was necessary to inhibit oxidation, at $220 \text{ }^\circ\text{C}$ for 12 h. The rationale for use of an argon atmosphere during sintering is as follows. Samples sintered in argon showed little or no oxidation, indicated by a color change of the surface as well as severe embrittlement, even after extended sintering periods. For hot pressing, the entire steel die was placed on a hot plate and heated to $200 \text{ }^\circ\text{C}$ and then pressed for 5 min, after which the die was removed from the press and allowed to air cool before removal of the compact. Hot-pressed specimens showed little oxidation.

Both cold and hot pressing (with the aforementioned 15–20 g powder) produced thin slabs approximately $50 \text{ mm} \times 12 \text{ mm} \times 3\text{--}5 \text{ mm}$ thick. Out of these slabs, 4–5 strips were cut out for testing using a low-speed abrasive diamond saw.

Samples for optical micrographs were potted in a two-part epoxy, and pucks were wet-ground using silica sandpaper, with coarse polishing done using a $1.0\text{-}\mu\text{m}$ diamond paste and fine polishing using a $0.03\text{--}0.06 \mu\text{m}$ colloidal silica solution. After polishing, some samples were etched by immersion in a solution of 100 ml ethyl alcohol and 3 ml HCl ⁷ for 45 s. Micrographs were taken using an optical microscope (Nikon Eclipse ME600, Mellville, NY) with a digital camera (Diagnostic Instruments, SPOT model #2.2.1, St. Sterling Heights, MI) and image capturing system (Metamorph 5.0r2, Universal Imaging Corp., Sunnyvale, CA) on a PC.

A microscope heating stage was built by gluing a large glass microscope slide ($5 \times 7.6 \text{ cm}$) onto a 3-in.-diameter disk of Omegalux SRFR heating tape (Omega, Stamford, CT) and an aluminum ($5 \times 7.6 \times 0.3 \text{ cm}$) plate to the other side (Fig. 3). A variable alternating current (ac) power supply was used to manually regulate temperature. Sample temperature was measured using a type-K (Omega) thermocouple inserted into a drilled access hole such that the thermocouple tip was just under the surface and in contact with the composite. The stage was placed onto the microscope slide holder, glass side down, and a sample puck was placed in the middle of the aluminum plate. Using a magnification of $200\times$ and polarized light, a section of the composite containing a large number of VO_2 inclusions was chosen for inspection, and pictures were taken of the high and low-temperature phases, as well as movies of the dynamic transition.

B. Experimental evaluation of composites

Specimens were tested in torsion using broadband viscoelastic spectroscopy (BVS) as outlined by Lee et al.⁸ with refinements to the temperature control and added

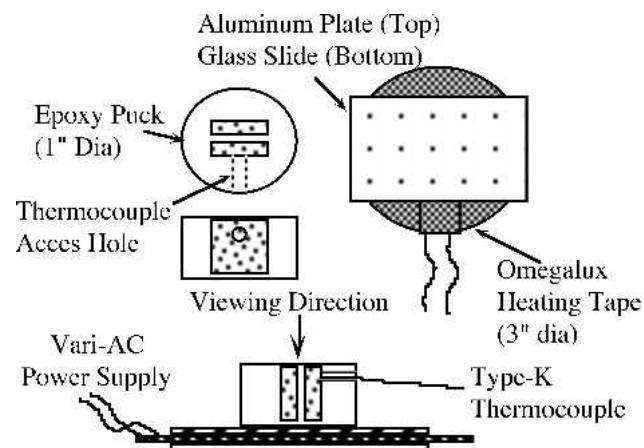


FIG. 3. Heating stage and specimen schematic for microscopy studies.

ability to measure slow, large-amplitude free end deflections of the cantilevered specimen. Figure 4 shows a schematic representation of the test setup. Samarium-cobalt magnets were glued to the specimen using Micro Measurements MBond 610 strain gage cement (Raleigh, NC) according to the curing and pressure schedule given in the instructions. The fixed end of the sample was mechanically clamped by tungsten adapters and set screws. Tests were conducted at 100 Hz, well below the resonance of the specimens, and heated via a resistive micro-tube furnace wound with Ni-Cr heating wire. Heating/cooling rates were on the order of 2 °C/min, with specific rates indicated in the figures. Lock-in amplifier sampling rates were 2 Hz, with a time constant of 30 ms. Sample temperature was measured using a type-K (Omega) thermocouple attached to the base of the sample; its voltage was recorded by a digital oscilloscope.

Internal friction ($\tan \delta$) and shear modulus measurements were taken using a Stanford Research Systems lock-in amplifier (SR850 DSP, Sunnyvale, CA) by measuring the phase angle between the sinusoidal torque and displacement signals as well as signal amplitude. Deflections of the free end of the cantilevered specimen due to any slow effects of material instability, were measured by a wide angle, 2 axis photodiode position sensor (Pacific Silicon Sensor Inc. DL100-7PCBA, Westlake, CA) with a detector area of 1 cm². This was accomplished by splitting off a portion of the laser beam and recording the detector output voltage with a digital oscilloscope for the horizontal (torsion) and vertical (bending) directions. Studies of stability of a 5% composite are reported elsewhere.⁹

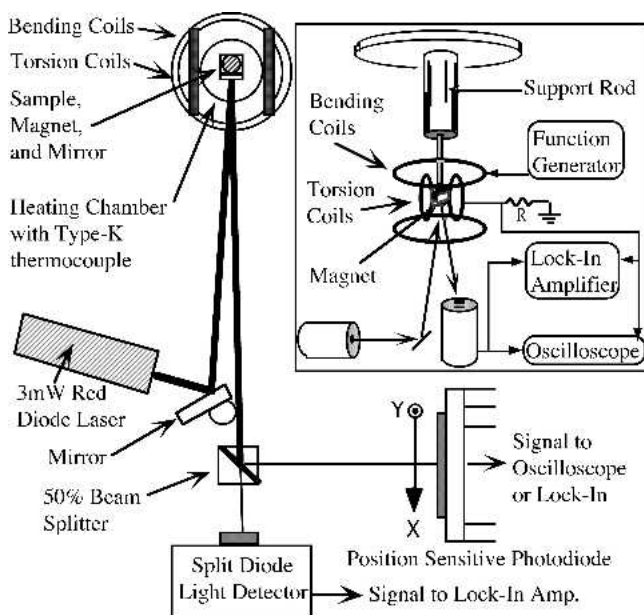
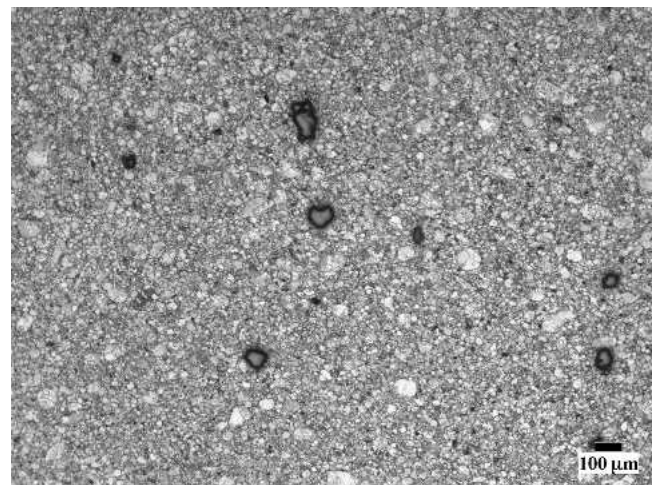


FIG. 4. Schematic illustration of the BVS viscoelastic test setup: (left) top view of configuration with large deformation capability and (inset) perspective view.

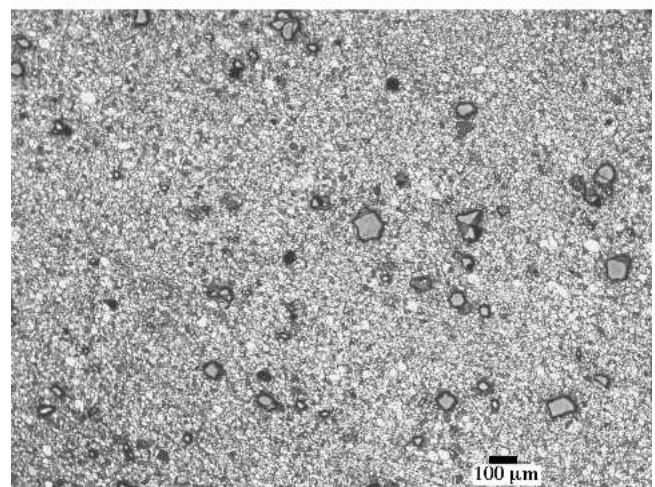
III. RESULTS

A. Microstructural analysis

Optical analysis of the consolidated and sintered powders revealed that the technique used was able to repeatedly achieve particle dispersions of the desired inclusion volume fractions (Figs. 5–7). Figure 5 shows low-magnification optical micrographs of dispersions in 1 and 5 vol% VO₂-Sn composites. However, due to low VO₂ volume fractions and large particle sizes, these dispersions were not homogeneous, especially in 0.5 vol% VO₂-Sn composites. For instance, Fig. 6(b) shows three large particles clustered together in a 0.5 vol% VO₂-Sn composite; in this case the local volume fraction is decidedly much higher than the nominal volume fraction of the bulk composite. No efforts were made to reduce particle size to better disperse the available particle volume in a more uniform manner.



(a)



(b)

FIG. 5. Low-magnification micrographs showing VO₂ particle dispersions in (a) 1 vol% and (b) 5 vol% VO₂-Sn specimens produced through powder metallurgy. VO₂ particles are the dark gray inclusions.

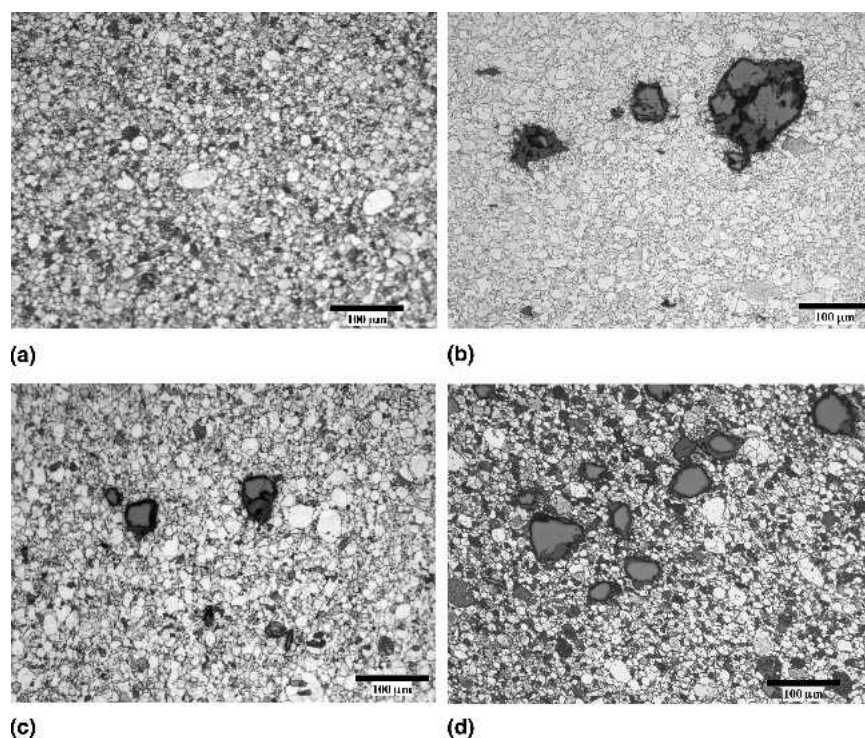


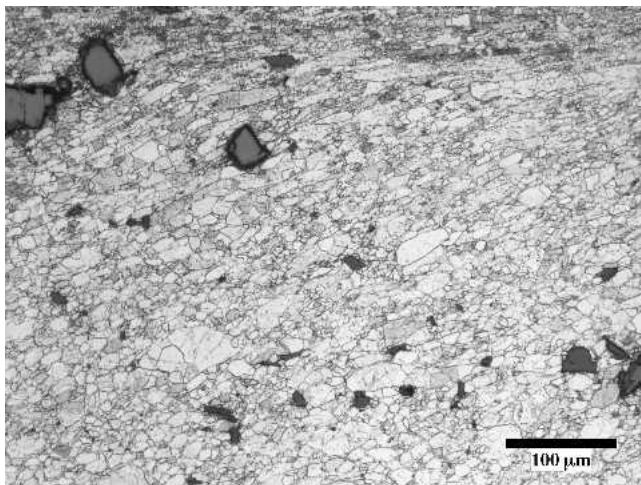
FIG. 6. Micrographs of (a) 0 vol%, (b) 0.5 vol%, (c) 1 vol%, and (d) 5 vol% VO_2 -Sn specimens produced through the powder metallurgy technique used in this study. VO_2 particles are the dark gray inclusions. These samples were cold pressed at 180 mPa, sintered in argon at 210 °C for 12 h.

With regard to composite microstructure, Fig. 6 shows four micrographs of composites prepared through cold pressing and sintering in argon atmospheres. The interiors of the cross sections displayed similar tin grain sizes for the four inclusion volume fractions shown (0, 0.5, 1, and 5 vol%). Using the linear intercept method,⁷ average grain sizes were measured to be about 10 μm . However, the grains are not equiaxed throughout any particular cross section. Abnormal grain growth and varying rates of recrystallization of the tin matrix were observed in all specimens. For example, Fig. 7 shows thin, elongated grains near the free surface and around VO_2 inclusions in a 5 vol% VO_2 -Sn composite. Elongated grains are most likely a result of the heterogeneous stress state evolved during the initial powder consolidation¹⁰ since the applied pressure exceeds the yield point of tin. Large-scale recrystallization may have been suppressed by entrapped gas porosity and VO_2 inclusions.

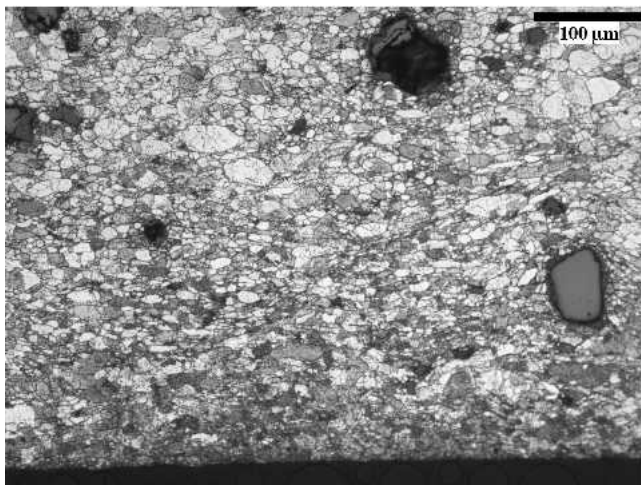
The phase transformation of the VO_2 inclusions can be examined visually at the surface of the composite due to thermochromatic characteristics of the phase transition.^{11,12} Above the transformation temperature, these inclusions are metallic and therefore opaque. Below the transformation they become translucent, which can easily be detected in an optical microscope. Accordingly, a transverse cross section of the 5 vol% VO_2 -Sn composite was observed in polarized, reflected light while being thermally cycled through a temperature

range of 25–120 °C. For the particular field of view shown in Fig. 8, no resolvable change was detected until the fifth thermal cycle, after which the band structure shown in Fig. 8(b) developed upon cooling. Further cycles revealed that the transition temperature for heating occurred at about 56 °C. Abrupt reversal of the entire band structure occurred in each particle over a range of only 1 or 2 °C. In contrast, upon cooling nucleation and advancement of band fronts were observed in larger inclusions, with faster evolution in the smaller inclusions. Band formation occurred over a temperature window of about 5–7 °C. Even though band formation was seen in some of the inclusions, signs of transformation were observed in inclusions that did not form bands. For example, in Fig. 8, the largest and rightmost inclusion, indicated by the double arrow, displayed no band formation even after seven thermal cycles. However, a reaction front that spanned the entire exposed surface of the particle was observed but was only detectable as a subtle shift in particle contrast. No macroscopic changes were observed in the tin matrix during these tests.

In summary, optical microscopy reveals the following: (i) dispersions of VO_2 particles are achieved but are not homogenous, especially in low volume fraction composites; (ii) microstructures have varying residual grain structures; (iii) the transformation characteristics are variable in each inclusion; and (iv) transformations, indicated by interparticle band formation and contrast



(a)



(b)

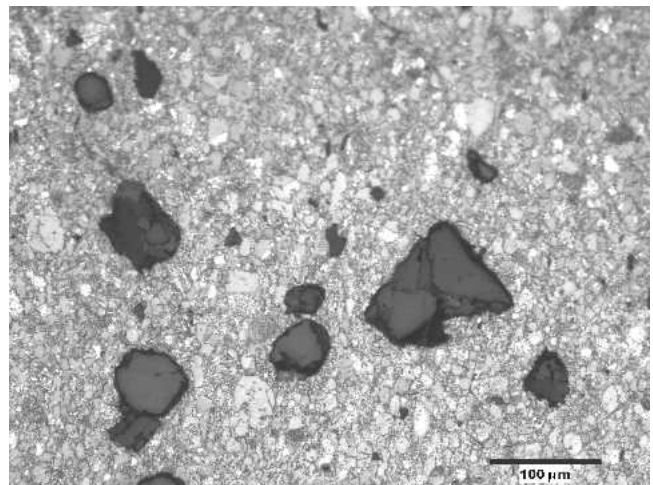
FIG. 7. Elongated grains from uniaxial pressing powder compaction (from top of image). These micrographs are from two different 5 vol% VO₂-Sn samples. The free surface is near the top of (a) and at the bottom of (b).

change, do not occur until the composite has experienced several thermal cycles.

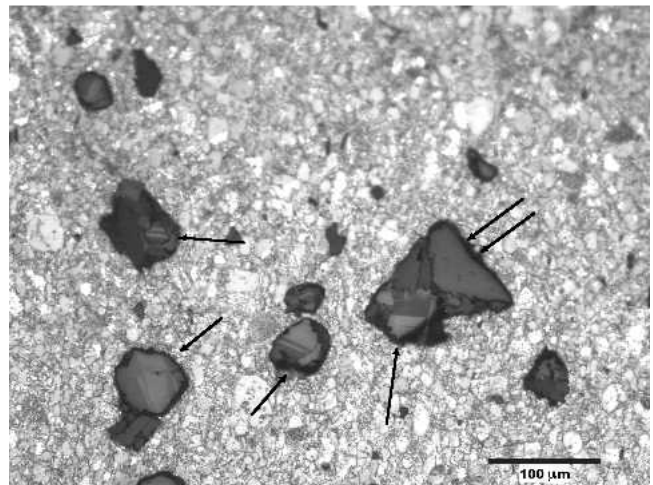
B. Mechanical properties

1. 0 vol% VO₂-Sn

Before conducting tests on the composites, experiments were conducted on a pure Sn sample prepared using powder metallurgy to achieve baseline values for $\tan \delta$ and the shear and Young's modulus. It was found that the pure Sn specimens produced through powder metallurgy had a room temperature $\tan \delta$ of 0.015 at 100 Hz, which is slightly less than the 0.02 of the cast specimens.⁵ $\tan \delta$ for the pure Sn showed a weak, linear temperature dependence increasing to 0.03 at 120 °C.



(a)



(b)

FIG. 8. Development of bands in VO₂ inclusions, inside a composite, when cooled from a temperature of (a) 75 °C to (b) 60 °C. Single arrows in (b) point out band formation in some of the larger particles. The double arrow indicates a particle which did not form bands but displayed a subtle change in contrast.

2. 1 vol% VO₂-Sn

A detailed view of the behavior of a pressed (powder metallurgy) 1 vol% VO₂-Sn composite is shown in Fig. 9. In the results in Fig. 9, a single, well defined, broad peak was observed in $\tan \delta$. Nine experimental runs are shown in which it is clear that the peak shifts up in temperature with successive thermal cycling. This was true for every cycle except run #4, which experienced a faster cooling rate than the other runs. The peak is not visible in the first thermal cycle as it is presumably outside of the temperature range tested. The hump in $\tan \delta$ is, in general, about 5 °C wide. The peak damping 0.04 is about 2.5 times the baseline room temperature damping of 0.015. This peak is also comparable to the maximum damping observed by Zhang et al.¹³ at a similar

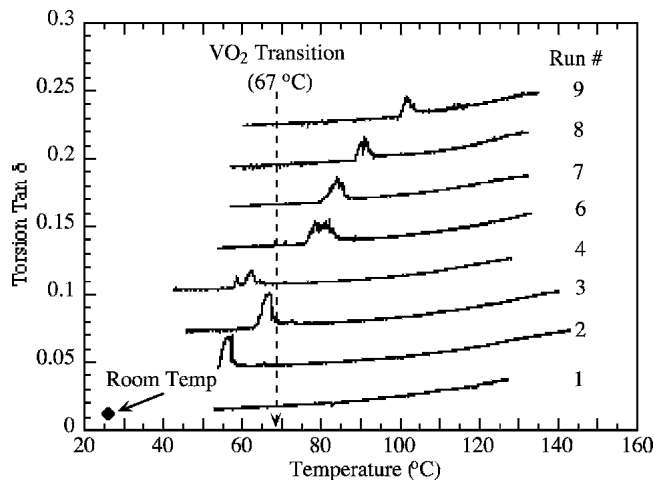


FIG. 9. Broad peaks in $\tan \delta$ observed in a 1 vol% VO_2 -Sn powder metallurgy sample. Nine cooling runs are shown. For the purpose of clarity, each successive curve beyond run #1 is shifted vertically by increments of 0.03. Data for run #5 was lost.

cooling rate for pure VO_2 , even though the present composite contains only 1% VO_2 by volume.

This particular specimen exhibited a slight transition in the shear modulus in the same temperature range as the broad damping peak. A shoulder (or step-up) in the shear modulus was observed which shifted along with the damping peak. In general, no sharp peaks were observed in any of the tested composites.

Figure 10 shows four experimental runs from a series of eight thermal cycles conducted on another 1 vol% VO_2 -Sn composite. This composite displayed a set of discrete doublets over almost the entire temperature range for two thermal cycles. Here we define a doublet as an increase, immediate decrease and then a return to the

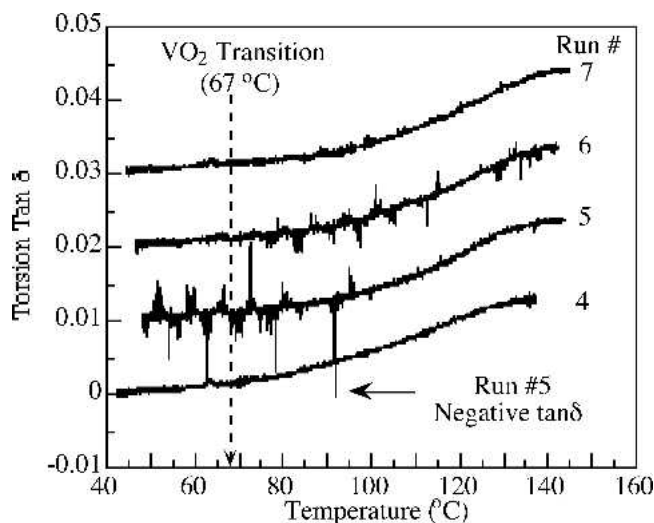


FIG. 10. 1 vol% hot pressed VO_2 -Sn sample displaying a set of discrete peaks in two experimental runs. Notice that one of the peaks goes negative momentarily. Curves are shifted vertically by increments of 0.01, with run #5 unshifted.

baseline damping. As shown in Fig. 10, thermal cycles 5 and 6 produced resolvable doublets in damping, whereas previous cycles displayed some small perturbations, and successive cycles showed no anomalous behavior. Observe that one of the doublets momentarily becomes negative during the 5th cooling cycle.

3. 0.5 vol% VO_2 -Sn

Figure 11 shows the third experimental run from series of five runs conducted on a 0.5 vol% VO_2 -Sn specimen tested in torsion as it was repeatedly cooled over temperature range of 140–60 °C. In the temperature range shown, a set of two damping doublets displayed an increase of almost a factor of two over the baseline $\tan \delta$ of 0.03 at 130 °C (see inset Fig. 11). Though the observed doublets in Figs. 10 and 11 display characteristics similar to the response of the cast composite seen in Fig. 2, this behavior is markedly different in that the anomalies occur over a wide temperature range, instead of just 1 °C, and that several anomalies exist and not a single event. Another variation on the behavior observed in the present composites is shown by three curves from a series of five cooling runs on a 0.5 vol% VO_2 -Sn sample (Fig. 12), which displayed what appear to be square offsets in $\tan \delta$. These offsets appeared in the second experimental run and dissipated by the fifth.

IV. DISCUSSION

A. Significance of processing and volume fraction on material behavior

Table I summarizes the general types of observed internal friction ($\tan \delta$) responses seen for all volume

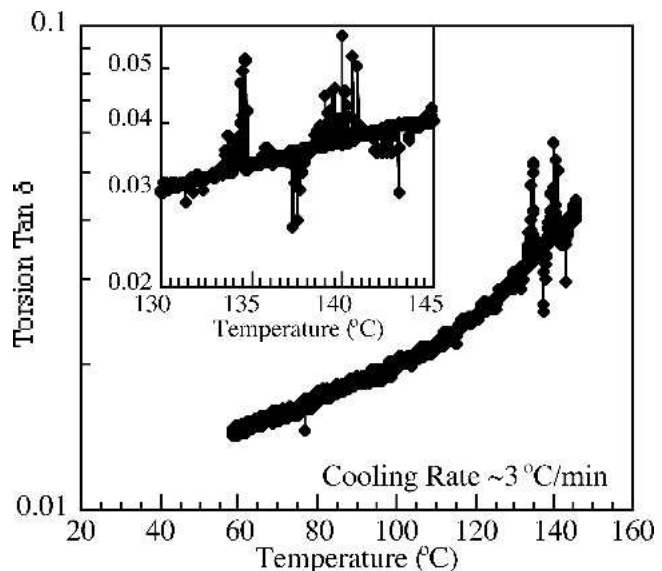


FIG. 11. 0.5 vol% VO_2 -Sn sample displaying a set of doublets, well above the usual transformation temperature. (Inset) shows an expanded scale around the anomalous behavior.

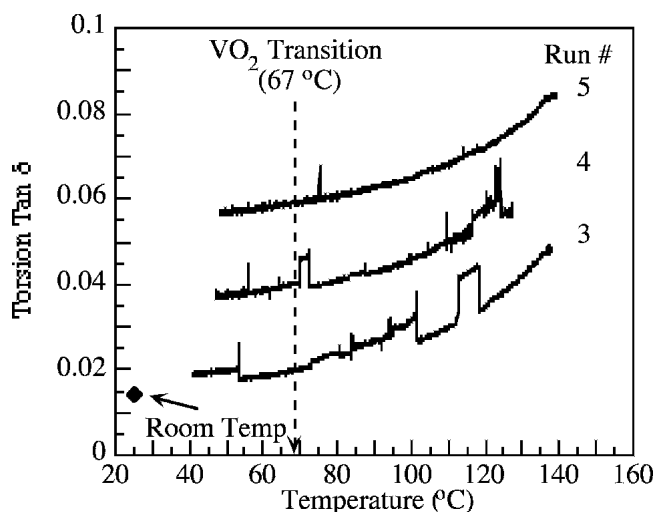


FIG. 12. 0.5 vol% VO₂-Sn sample displaying offset in tan δ . Offsets appeared during the second cooling run (not shown) and disappeared after the fourth run. Curves are shifted beyond run #3 by increments of 0.02.

fractions of VO₂ tested. Four general categories were witnessed: samples which displayed (i) no anomalies, (ii) doublets, (iii) unstable phase jitter, and (iv) large peaks or small humps. It must be noted that data from the 5 vol% VO₂ samples, which were predicted to be unstable, have been reported elsewhere;⁹ the data reported here for 5 vol% VO₂ specimens are included only for comparison to the stable volume fractions. We presume, however, that instability can occur in nominally stable compositions if the local volume fraction for a given specimen is higher than the bulk from which it was made due to large particle sizes and a heterogeneous particle dispersion. Another important point to note is the greater incidence of peaks and humps with increasing volume fraction until the stability limit is reached. The intensity and width of these peaks are governed by internal variables other than the composite volume fraction.

Figure 13 illustrates the contrast between the observed material responses of the cast VO₂-Sn composites and those of the VO₂-Sn composites made through powder metallurgy. In general, the damping peaks observed in the pressed and sintered composites were broader in the thermal domain and lower in intensity than the damping

TABLE I. Summary of observed responses in sample tan δ over the tested volume fractions.

Vol% VO ₂	Total tested	Anomalies	Doublets	Phase jitter	Peaks or humps
0	3	0	0	0	0
0.5	6	3	1	1	1
1	8	6	1	2	3
5 ^a	9	7	3	2	1

^aData for 5 vol% VO₂ comes from Ref. 9.

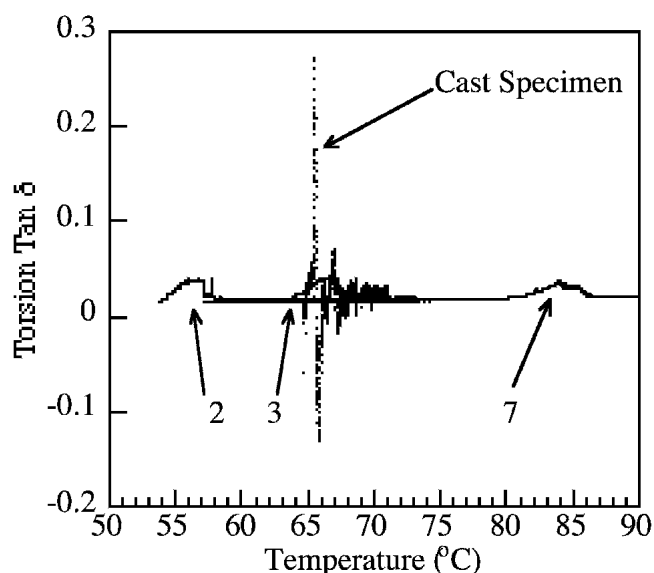


FIG. 13. Comparisons of the broad humps in tan δ seen in the present 1 vol% VO₂-Sn composites to the original results for a cast composite by Lakes et al. Thermal cycles #2, #3, and #7 are shown from Fig. 9.

peaks reported from the cast composites. No sharp anomalies in composite stiffness were observed in the composites made through powder metallurgy. In some cases, the internal friction is broadened, not into a single hump, but into a series of discrete peaks or doublets. Furthermore, it is inferred from both mechanical and optical observations that the state of the internal structure is highly dynamic. This inference is based on the thermal cycle dependence, both in peak amplitude as well as incident temperature, on the internal friction behavior seen in all powder metallurgy samples displaying any kind of internal friction anomaly. In contrast, no peak shifting was reported in the cast specimens; however, the cast composites were tested over a very narrow temperature window. Identification of the internal variable, or variables, controlling the dynamic nature of the present composite's range of mechanical behavior is not immediately clear through analysis of the internal friction data.

B. Mechanisms governing distribution of behavior and transformation temperature

Nominally, observation of negative stiffness behavior should concur with the reported abrupt, reversible ferroelastic phase transition occurring at 68 °C. However, inference of the internal friction data, in conjunction with direct observation of the optical transition, leads to the conclusion that the phase transition in the composite material occurs over a much broader range than expected and does not reversibly occur at 67 °C. Below, we consider several possible factors that might, in principle, lead to broadening and shifting of the transformation.

The first mechanism to consider is stress. It is well

known that phase transition temperatures are thermodynamic functions of pressure, such as the Clausius–Clapeyron equation. Salje¹⁴ states that the critical temperature of a ferroelastic phase transition can be broadened by introducing a heterogeneous elastic stress, resulting in a broadening of the phase transition from a single well defined temperature to a range of temperature spanning tens of degrees. Considering the specific behavior of VO₂, the stress (*S*) dependence along the crystal's *c* axis on the transition temperature (*T_c*) has been reported as $(\delta S/\delta T_c) = -1.2 \times 10^3$ K/bar (or 1.2×10^8 K/Pa), with stresses in the other crystallographic directions spanning the hysteresis width.¹⁵ Other authors also report similar stress dependencies in thin films.^{16,17} With this magnitude of sensitivity, stresses on the order of 100 MPa are required to shift the ferroelastic transition temperature of VO₂ 1 K. Considering the results shown in Fig. 11, a stress change of almost 4000 MPa would be required to shift the peak over the 45° window. However, stresses of even a few MPa cannot be maintained on the inclusions by the Sn matrix given the creep strength^{18,19} and yield point of Sn, even at extremely high strain rates. Thus, shifts of the transformation temperature are most likely not due to residual stresses from processing nor stresses imposed by the tin matrix during inclusion transformation.

Another factor for consideration is the richness of valence states available to vanadium in the vanadium–oxygen system. Vanadium has the ability to take many valence states resulting in the formation of a large number of different oxides, directly evident from the phase diagram presented by Griffiths and Eastwood.²⁰ Sensitivity to oxygen partial pressure and other preparation parameters can lead to single crystals with small minority phases of other vanadium-based oxides or morphological defect structures,^{19,21} and in this regard a monotonic 10 °C decrease in transition temperature for oxygen-deficient VO₂ has been reported.¹⁹ Furthermore, depression of the transition temperature can be accomplished by doping with tungsten, molybdenum, niobium, and rhenium.¹² It is presumed that distributions in powder stoichiometry or impurity concentration could give rise to a distribution of peaks occurring at different temperatures. However, this would not explain peak temperature shifting as a function of thermal cycling.

Observed dynamic temperature shifting of the damping peaks could arise through a possible sensitivity of VO₂ to small changes in stoichiometry by reaction with the tin matrix. It might be possible that oxygen or tin could diffuse into surface regions of the inclusions during sintering and subsequent thermal cycling, altering the properties of the reacted region. Tin also forms a rutile oxide, easily substituting for surface vanadium and altering the local electronic state and lattice spacings. Deviations from the nominal lattice spacing in pure,

stoichiometric VO₂ could push portions of a granule closer to the metallic or insulator state and change the nucleation barrier.¹⁷ Smaller VO₂ granules will be more susceptible to such effects in view of their larger ratio of surface to volume.

Lastly, it is possible that the inclusion transformation is dependent on the structure of the VO₂–tin interface. As previously mentioned, negative stiffness behavior is allowed only in a constrained system, which is provided by the tin matrix. Loss of hard constraints on the negative stiffness phase leads to unsuppressed “snap-through” of the negative stiffness inclusions and therefore loss of any stiffening effects. Changes in interfacial structure are suggested by the decrease in amplitude of the observed damping peaks after successive thermal cycles. Loss of inclusion constraint could also arise from surface diffusion of tin.

C. Analysis using a distribution of negative moduli in composite theory

As previously mentioned, negative stiffness particulate composite performance can be predicted through use of the Hashin–Shtrikman shear modulus formula by letting the ratio of inclusion shear modulus to matrix shear modulus become progressively more negative. This analysis requires the assumption of a baseline $\tan \delta$ for the matrix, as well as volume fractions of each constituent. From the results for pure Sn made through powder metallurgy, a $\tan \delta$ of 0.015 was assumed for the matrix at the transition temperature. A further and highly restrictive assumption is that all of the inclusions are identical. In other words, it was assumed that each VO₂ inclusion had the same negative modulus and that each inclusion transformed at the same time. This assumption resulted in the prediction of a single, sharp anomalous event in $\tan \delta$ and a doublet in shear modulus. However, the results reported in this work, namely observation of broad internal friction peaks and variation in the observed optical behavior of the inclusions, suggest it is expedient to analytically consider a distribution of inclusion stiffness values. This distribution needs to be reflected in the theoretical consideration.

The material behaviors in Fig. 14 were calculated using Eq. (2) for a single negative modulus and Eqs. (3) and (4) for a discrete distribution of negative moduli (here, $N = 20$). Comparison of the predicted theoretical response of Fig. 14 with the actual observed material responses in Fig. 13 shows that the basic assumptions behind the theory are valid, and that indeed a distribution of discrete negative stiffness moduli is responsible for the observed behavior in this study. Even though the qualitative character of the response can be predicted, the actual structural parameters leading to the overall form of the response and the evolution of this response with thermal cycling are not forthcoming from Eqs. (2)–(4).

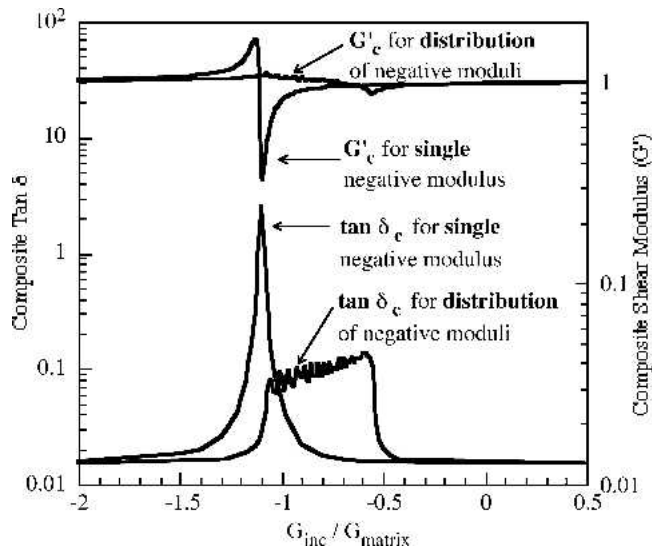


FIG. 14. Theoretical difference between predicted material response between a 0.5 vol% composite containing inclusions with a single negative modulus and that with a distribution of negative moduli.

$$G_L = G_2 + \frac{V_1}{\frac{1}{G_1 - G_2} + \frac{6(K_2 + 2G_2)V_2}{5(3K_2 + 4G_2)G_2}}, \quad (2)$$

$$G_L = G_2 + \sum_{k=1}^N \frac{V_1}{\frac{1}{\{G_{1k}\} - G_2} + \frac{6(K_2 + 2G_2)V_2}{5(3K_2 + 4G_2)G_2}} \frac{1}{N}, \quad (3)$$

$$\{G_{1k}\} = G_1(1 + .05k) \quad (4)$$

Here G_L is the lower bound from the Hashin–Shtrikman formula, G_2 , K_2 , V_2 are the matrix shear modulus, bulk modulus, and volume fraction respectively, and G_1 and V_1 are the inclusion shear modulus and volume fraction, respectively.

As for possible application in high-performance damping layers, broadening of the damping peak is certainly beneficial; however, the dependence on thermal cycling is not helpful and would have to be removed for these composites to be of use as practical damping materials.

V. CONCLUSIONS

Powder metallurgy as a processing route for composites with negative stiffness inclusions is successful in that, with the current procedure, this method has the ability to routinely result in a bulk material with a dispersed second phase of ceramic inclusions. However, the internal friction behavior occupies a broader range of temperature and detailed mechanical response than in the cast composites studied previously.

Observed anomalies in the mechanical properties of the composites studied are consistent with the predicted negative stiffness behavior of the VO_2 inclusions being

partially stabilized by the positive stiffness tin matrix. However, these anomalies had a much broader and shallower character than the sharp peak previously observed in the cast composites. Moreover, sets of peaks were obtained in some composites. Powder metallurgy also produced composites with responses that depended on thermal cycling, both in the amplitude of the response and location of the anomalies in the temperature domain. The difference in behaviors between the cast composites and those made through powder metallurgy are attributed to a distribution of inclusion negative stiffness moduli in the latter material. This distribution can be qualitatively inferred from composite theory by allowing a discrete series of negative moduli in the Hashin–Shtrikman shear modulus formula. The composite theory thus far does not yet capture sufficient physics to predict thermal cycling or other effects observed.

REFERENCES

1. R.S. Lakes: Foam structures with a negative Poisson's ratio. *Science* **235**, 1038 (1987).
2. R.S. Lakes: Extreme damping in compliant composites with a negative-stiffness phase. *Philos. Mag. Lett.* **81**, 95 (2001).
3. R.S. Lakes and W.J. Drugan: Dramatically stiffer elastic composite materials due to a negative stiffness phase? *J. Mech. Phys. Solids* **50**, 979 (2002).
4. E.K.H. Salje: *Phase Transformations in Ferroelastic and Coelastic Crystals*, (Cambridge University Press, Cambridge, U.K., 1990), p. 5.
5. R.S. Lakes, T. Lee, A. Bersie, and Y.C. Wang: Extreme damping in composite materials with negative-stiffness inclusions. *Nature* **410**, 565 (2001).
6. Y.C. Wang, M. Ludwigson, and R.S. Lakes: Deformation of extreme viscoelastic metals and composites. *Mater. Sci. Eng. A* **370**, 41 (2004).
7. G.F. Vander Voort: *Metallography Principles and Practices* (McGraw-Hill, New York, 1984), p. 691.
8. T. Lee, R.S. Lakes, and A. Lal: Resonant ultrasound spectroscopy for measurement of mechanical damping: Comparison with broadband viscoelastic spectroscopy. *Rev. Sci. Instrum.* **71**, 2855 (2000).
9. T. Jaglinski and R.S. Lakes: Anelastic instability in composites with negative stiffness inclusions. *Philos. Mag. Lett.* **84**, 803 (2004).
10. J.S. Hirschhorn: *Introduction to Powder Metallurgy* (American Powder Metallurgy Institute, New York, NY, 1969).
11. P. Jin and S. Tanemura: Formation and thermochromism of VO_2 films deposited by RF magnetron sputtering at low substrate temperature. *Jpn. J. Appl. Phys.* **33**, 1478 (1994).
12. C.G. Granqvist: Energy-efficient windows: Present and forthcoming technology, in *Materials Science for Solar Energy Conversion Systems*, edited by C.G. Granqvist (Pergamon Press, Oxford, U.K., 1991), pp. 106–167.
13. X.J. Zhang, Z.H. Yang, and P.C.W. Fung: Dissipation function of the first-order phase transformation in VO_2 ceramics by internal friction measurements. *Phys. Rev. B* **52**, 278 (1995).
14. E.K.H. Salje: *Phase Transformations in Ferroelastic and Coelastic Crystals* (Cambridge University Press, Cambridge, U.K., 1990), p. 33.
15. L.A. Ladd and W. Paul: Optical and transport properties of high quality crystals of V_2O_4 near the metallic transition temperature. *Solid State Commun.* **7**, 425 (1969).

16. J.M. Gregg and R.M. Bowman: The effect of applied strain on the resistance of VO₂ thin films. *Appl. Phys. Lett.* **71**, 3649 (1997).
17. K.Y. Tsai, T. Chin, H.D. Shieh, and C.H. Ma: Effect of as-deposited residual stress on transition temperatures of VO₂ thin films. *J. Mater. Res.* **19**, 2306 (2004).
18. R.J. McCabe and M.E. Fine: Creep of tin, Sb-solution-strengthened tin, and SbSn-precipitate-strengthened tin. *Metall. Mater. Trans.* **33A**, 1531 (2002).
19. P. Adeva, G. Caruana, O.A. Ruano, and M. Torralba: Microstructure and high temperature mechanical properties of tin. *Mater. Sci. Eng. A* **194**, 17 (1995).
20. C.H. Griffiths and H.K. Eastwood: Influence of stoichiometry on the metal-semiconductor transition in vanadium dioxide. *J. Appl. Phys.* **45**, 2201 (1974).
21. D. Maurer and A. Leue: Investigation of transition metal oxides by ultrasonic microscopy. *Mater. Sci. Eng. A* **370**, 440 (2004).